

# Platform Scattering Analysis of the Copernicus Imaging Microwave Radiometer

P. G. Nicolaci<sup>1</sup>, C. Cappellin<sup>1</sup>, R. Mizzoni<sup>2</sup>, V. Lubrano<sup>3</sup>, S. Contu<sup>3</sup>, B. Fiorelli<sup>4</sup>

<sup>1</sup> TICRA, Copenhagen, Denmark, cc@ticra.com

<sup>2</sup> Independent Consultant for TASI on CIMR, Rome, Italy

<sup>3</sup> Thales Alenia Space Italia, Rome, Italy

<sup>4</sup> ESA ESTEC, Noordwijk, The Netherlands

**Abstract**— The Copernicus Microwave Imaging Radiometer (CIMR) employs a 7.1 m conical scanning mesh reflector antenna rotating at 7.8 rpm that operates from L to Ka band. Demanding radiometric accuracies and sensitivities at few tenths of a Kelvin at high spatial resolution are targeted for the instrument. These require a high accuracy in the characterisation and modelling of the antenna pattern over  $4\pi$ , considering any nearby scattering structure and/or any potential multipath due to the antenna installation over the S/C. Moreover, the quantification of the fractional power hitting each scatterer entering by reciprocity into the feeds is also of primary importance, since it can bias the antenna temperature. A platform scattering analysis of the reflector antenna on the CIMR satellite was thus undertaken for a subset of feeds at L, C, X, K, and Ka bands. In this paper we describe the analyses done and summarise the effect of these scatters over the antenna RF performances.

**Index Terms**—CIMR, Satellite Scattering, Scattering Power Budget, Antenna Model, MoM/MFLMM, LDR

## I. INTRODUCTION

The Copernicus Microwave Imaging Mission (CIMR) will employ a conical scanning passive microwave radiometer to measure from an average altitude of 832 km sea ice concentration and sea surface temperature over the Arctic regions and the world-wide oceans. The radiometer antenna is an array-fed offset Large Deployable Reflector (LDR) in light mesh technology of  $\sim 7.1$  m in diameter, operating from 1.4 GHz to 36.5 GHz. The antenna is fed through a focal plane feed cluster of 13 feeds constituted by one L band dual polarized array of patch excited cup elements, four dual band dual polarized self diplexed feeds operating in C and X band and eight dual band, dual polarized self diplexed feeds operating at Ku and Ka band.

The CIMR instrument shall comply with stringent requirements for its radiometric accuracies and sensitivities at all channels. This implies a meticulous knowledge and stability of the antenna temperature and its beam efficiency, including for geolocalization high RF beam(s) pointing accuracies [1],[2]. The whole antenna is spinning at 7.8 rpm, making it impossible to measure the reflector profile and RF patterns on ground under rotation. Moreover, the reflector antenna, its boom, and the satellite body will affect the performance of the standalone reflector antenna. The

complex mesh reflector technology and total geometrical size prevents radiated payload RF measurement over the S/C with the boom and LDR deployed in flight configuration. Therefore, it is of paramount importance to develop very accurate RF models of the CIMR antenna and its satellite already in the design phase and use these for the in-flight performance predictions throughout the project. Experience from previous missions, see for example the platform scattering modelling done for Exomars [3], has shown that this can be done with commercial software tools specifically developed for space applications.

The purpose of the present paper is to evaluate the effect on the pattern characteristics given by the antenna boom, truss, crate, and satellite body including solar panels, relative to the performance given by the standalone reflector.

The paper is organised as follows: Section II describes the satellite platform RF model and the pattern characteristics under investigation, Section III reports the scattering analyses results in terms of beam efficiency variation and scattered power budget. Conclusions are finally outlined in Section IV.

## II. CIMR SATELLITE PLATFORM MODEL

Ideally the antenna would capture only the signal coming from the scene under observation. Unfortunately, there are several stray fields that can bias the scene. The effects of the LDR scatterers like the boom, the truss, the crate, and the installation on the S/C produce two undesirable effects:

- The modification of the far-field radiation pattern over  $4\pi$ , with consequences on the side-lobes and the beam efficiency accuracy/knowledge.
- The modification of the antenna temperature due to the nearby obstacles whose emissivity can give a second order contribution to the antenna temperature.

Regarding the first effect, the  $4\pi$  antenna pattern requires a full wave modelling of all antenna parts (e.g. truss, boom, crate) and the S/C body with solar panels. Concerning the second effect, the fractional power from any scatterer to the antenna feed must be quantified.

At Ka-band the challenges of the full wave modelling are especially evident. The computational effort was managed using the ESTEAM software product [4] within the TICRA

Tools suite. ESTEAM is based on a higher order MoM/MFLMM formulation, that is adopted for the entire CIMR antenna/platform EM modelling. This allowed us to obtain very accurate analyses, at affordable computational time and RAM effort as highlighted in Table 1. All the simulations were run on a server machine HPE ProLiant DL380 Gen 10, Intel Xeon Gold 5218 CPU, with 64 logical cores and 1536 GB memory RAM.

TABLE 1: MoM/MFLMM MEMORY RESOURCE VS FREQUENCY

Band	MoM/MFLMM Memory RAM [GB]	
	Antenna stand alone	Full satellite
L band	0.76	16
C band	16	52
X band	35	82
K band	92	200
Ka band	220	689

### A. RF model setup

The CIMR satellite platform is constituted by five macro scatterers, as illustrated in Fig. 1:

1. faceted reflector surface
2. boom
3. truss
4. crate and focal plane
5. SC/body and solar panels

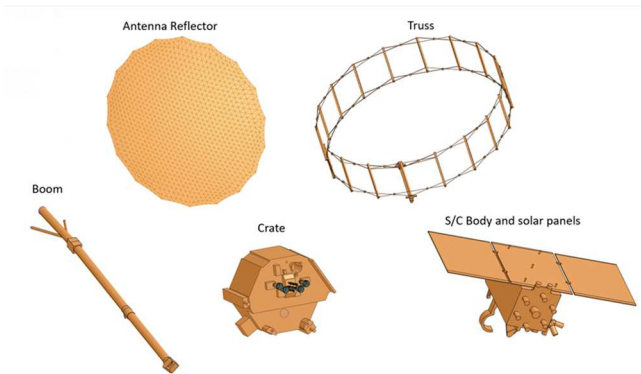


Fig. 1. CIMR satellite macro scatterers.

All scatterers are provided by TAS-I by means of CAD files and imported by TICRA in TICRA Tools for electromagnetic analyses. Fig. 2 depicts the CIMR focal plane with the radiating elements.

At L-band the feeder is an array of 12 radiating cup elements which is modelled by means of the full sphere pattern files provided by TAS-I. At C/X band and the K/Ka, the feeds internal profiles were provided by TAS-I, imported in the CHAMP 3D software in TICRA Tools and analyzed with mode matching for the horn interior and Body-of-Revolution (BoR) MoM for the horn exterior.

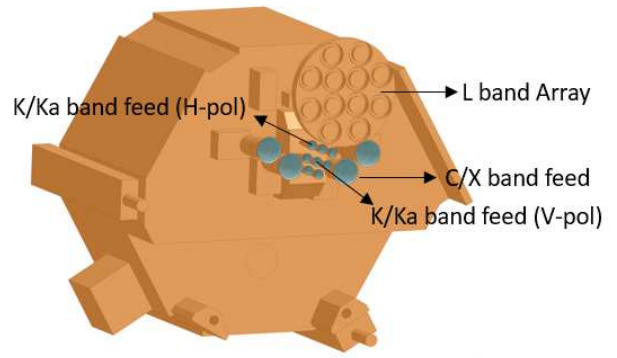


Fig. 2. Crate with the CIMR feeds.

The analyses were carried out at L, C, X, K, and Ka band over a subset of feeds in vertical and/or horizontal polarisation, as highlighted in Fig. 2 and Table 2. For the C/X band, only one feed close to the focal point was used for the scattering analyses, while the central feed and the most scanned feed were used for the analyses at K/Ka band (the closest to the antenna focal point in V-pol and the most scanned one in H-pol).

TABLE 2: SUBSET OF FOCAL PLANE FEEDS CONSIDERED IN THE PLATFORM SCATTERING MODELING

Focal Plane Feed Array: subset of elements, frequencies and polarisations used in the platform EM scattering analyses			
Band	Feed /channel identification	Frequency (GHz)	Polarisation
L band	L1-H&V	1.4	H&V
C band	C1-H&V	6.675	H&V
X band	X1-H&V	10.6	H&V
K band	K4 V-K8 H	18.6	K8 (H), K4 (V)
Ka band	Ka4 V-Ka8 H	36.5	K8 (H), K4(V)

As an example, Fig. 3 shows the MoM mesh of the full system at L-band; the green objects are perfect conducting closed objects while the brown objects represent open perfect conducting objects. All scatterers are modelled as perfect electrical conductors (PEC).

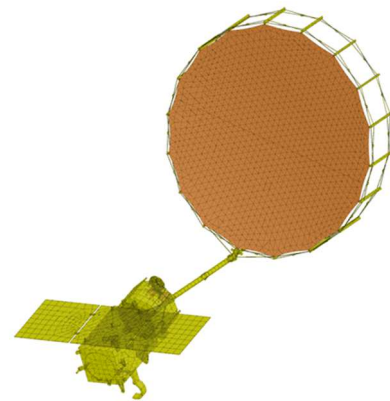


Fig. 3. CIMR satellite mesh at L-band; the green objects are perfect conducting closed objects while the brown ones represent open perfect conducting objects.

A plot of the currents induced on the full assembly at L-band is shown in Fig. 4

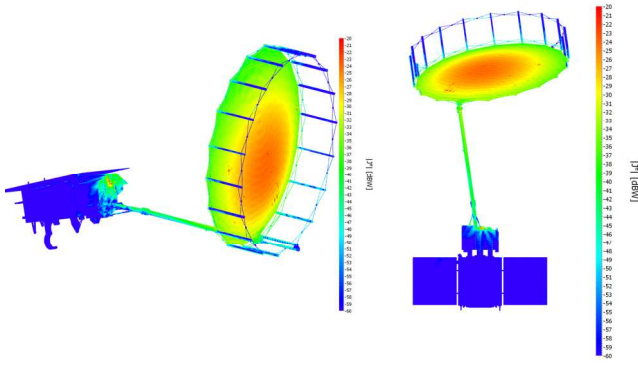


Fig. 4. Currents on the CIMR satellite at L-band.

### B. Pattern Characteristics Under Investigation

The scope of the scattering analyses is to evaluate the impact of each scatterer on the pattern characteristics which might impact the radiometer performance. The adopted procedure is based on an incremental approach, where a new scatterer is introduced in the model and a full wave analysis at each band is subsequently carried out. The starting point for the analyses is the reflector stand alone with the relative feed, which provide the so-called nominal performance. The pattern characteristics evaluated at each step are:

1. Beam pointing in the antenna reference system ( $U_p$ ,  $V_p$ )
2. Co-polar peak
3. Half Power Beamwidth (HPBW)
4. Main beam efficiency
5. Wide beam efficiency
6. Cross-polar power percentage

During the analyses it was found that the beam efficiency (BE) was the most sensitive parameter while the other pattern characteristics were not, or only marginally, affected by the additional scatterers (e.g. the worst case for maximum co-polar peak variation is around 0.13 dB at L-band).

It must be noted that the BE variation is strictly related to the variation of the co-polar peak, the HPBW and/or to the average sidelobe level over  $4\pi$  [5]. More explicitly, dB variation of the order of tenths in the co-polar peak can induce a non-negligible variation on the BE. For this reason, the next section is focused on the evaluation of the BE variation/stability and the scattering power budget.

### III. SCATTERING ANALYSES RESULTS

The RF simulations were performed in the ESTEAM software adding one scatterer at a time starting with the standalone antenna reflector and its primary feed. This approach allowed for quantification of the impact on the main beam RF performance of each scatterer and to estimate the incremental variation due to these scatterers' contributions.

### A. Beam Efficiencies

The main and wide BEs are calculated using the formula (1):

$$\eta = \frac{\int_0^{2\pi} \int_0^{\theta_1} (|E_{co}(\theta, \phi)|^2 + |E_{cx}(\theta, \phi)|^2) \sin \theta d\theta d\phi}{\int_0^{2\pi} \int_0^{\pi} (|E_{co}(\theta, \phi)|^2 + |E_{cx}(\theta, \phi)|^2) \sin \theta d\theta d\phi} = \frac{\int_0^{2\pi} \int_0^{\theta_1} (|E_{co}(\theta, \phi)|^2 + |E_{cx}(\theta, \phi)|^2) \sin \theta d\theta d\phi}{4\pi} \quad (1)$$

where  $\theta_1$  is  $2.5 * \theta_{3dB}$  for the main BE and  $3 * \theta_{3dB}$  for the wide BE.

Table 3 reports the BE performance of the nominal antenna, i.e., reflector alone, compared to the simulations that include all the macro scatterers, i.e., truss, boom, crate, S/C body, and solar panels at all CIMR bands.

TABLE 3: BEAM EFFICIENCY VS SCATTERING IN THE FULL BAND

Beam Efficiency Sensitivity vs Scatterers					
Band	Channel	Nominal V-pol [%]	Nominal H-pol [%]	Delta V-Pol [%]	Delta H-Pol [%]
L	L1-H&V	90.208	90.077	-1.223	2.878
C	C1-H&V	88.499	88.679	-0.723	-0.843
X	X1-H&V	94.917	95.111	0.724	0.285
K	K4 V-K8	95.750	92.585	-0.733	-0.355
Ka	Ka4 V-	97.170	93.845	-0.272	0.188

Legend:

Nominal=BE with standalone reflector

Delta=BE(nominal)-BE(all scatterers)

The major impact on the BE performance is seen in L- and C-bands and can be justified by the relatively higher primary reflector illumination aiming to guarantee the on-ground footprint as specified by the requirements. Ultimately the scatterers impact the nominal beam efficiency up to ~3% at L-band ~0.3% at Ka-band.

Table 4 provides details about which scatterer is the main contributor for the BE degradation at L-band.

TABLE 4: BEAM EFFICIENCY VS MAIN SCATTERERS AT L BAND

Beam efficiency at L band vs Scatterers				
Scatterer	BE V-pol [%]	BE H-pol [%]	Delta V-Pol [%]	Delta H-Pol [%]
Reflector stand alone	90.21	90.08	-	-
Reflector and Truss	90.13	89.97	0.079	0.11
Reflector, Truss and Boom	90.19	90.06	0.019	0.015
Reflector, Truss, Boom and Crate	91.48	87.25	-1.27	2.83
All scatterers	91.43	87.18	-1.25	2.92

Legend:

Delta=BE(nominal)-BE(included scatterers)

Nominal=BE with standalone reflector

All scatterers = Reflector, Truss, Boom and S/C with solar panels

It can be observed that the boom, truss, and S/C with solar panels have a negligible impact on the BE variation while the crate is the scatterer which gives the highest contribution. In addition, it is shown that the crate does not behave equivalently for the two orthogonal polarisations. This behaviour is similar at the other bands, though the analyses may not be fully exhaustive since they were carried out at only one channel frequency for each band.

### B. Scattering vs antenna rotation

Another undesirable dynamic contribution, to be absolutely prevented, is the interaction of the antenna under rotation with the solar panels, whose temperature can vary along the orbit. In case it is relevant, the instrument may be subject to pattern modification and antenna temperature variations with a period of 7.8 rpm with important consequences on antenna temperature, unless this error can be filtered in some way. To this end, the evaluation of the scattering when the antenna system rotates w.r.t the S/C and solar panels was carried out at the lowest band. Fig. 5 shows the S/C and solar panels scattered power at L-band for the H-pol as a function of the rotation angle. It can be appreciated that the scattered power is below -29 dB (around 0.001 in fractional power) and the variation under rotation is 0.00058, giving an almost negligible antenna temperature variation under rotation.

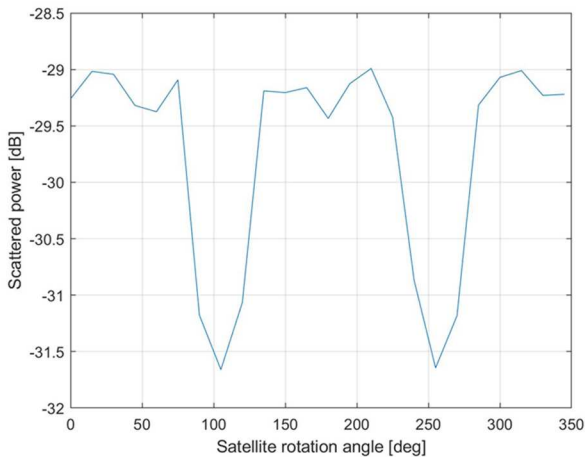


Fig. 5. CIMR L-band scattered power under rotation

### C. Scattering Power Budget

The scattering power budget is calculated to evaluate the amount of power scattered by each scatterer. As highlighted in [1], this power can alter the antenna temperature due to the scatter emissivity. Assuming  $\Delta P_i$  the fractional power scattered by the  $i$ -th scatterer, that would be the power entering into the feed due to the scatterer, the antenna temperature will be altered by a factor reported in (2):

$$\Delta T_{ANT,i} = \Delta P_i \varepsilon_i T_{S,i}^{physical} \quad (2)$$

where  $\varepsilon_i$  is the emissivity of the  $i$ -th scatterer at its physical temperature  $T_{S,i}^{physical}$ . The equation above clearly shows the

necessity to determine and minimise any  $\Delta P_i$  in order to characterise and minimise  $\Delta T_{ANT,i}$ .

The fractional power striking and radiated by each scatterer was calculated by taking the full wave simulations of Section A. In these simulations one scatterer is added at a time, computing then the difference pattern between two consecutive configurations, and finally integrating the scattered field in the full sphere to have the fractional power of the specific scatterer. Table 5 and Table 6 report the scattered power of each scatterer in the L, C and X bands for the V-pol and H-pol respectively.

TABLE 5: SCATTERED POWER BUDGET AT L, C, X BAND IN V-POL

Scattered power [dB]			
Scatterer	L band	C band	X band
Truss	-21.82	-20.43	-29.06
Boom	-25.41	-22.63	-23.49
Crate	-25.24	-25.28	-22.94
S/C and solar panels	-32.04	-35.82	-28.60
All scatterers	-19.54	-19.07	-20.80

TABLE 6: SCATTERED POWER BUDGET AT L, C, X BAND IN H-POL

Scattered power [dB]			
Scatterer	L band	C band	X band
Truss	-21.08	-20.48	-28.52
Boom	-26.91	-24.19	-28.18
Crate	-25.37	-24.77	-22.24
S/C and solar panels	-29.26	-35.56	-27.25
All scatterers	-19.6	-19.47	-22.21

It is seen that the objects which have a relevant contribution to the overall scattered power change with frequency and with polarisation.

Truss, boom, and crate are the most relevant scatterers in L and C bands. Regarding the boom, the difference between H-pol and V-pol can be reported as shown in Fig. 6. V-pol scattering is always higher, since it corresponds to the polarisation aligned along the boom direction.

At X-band the truss becomes negligible. This is because at this frequency the primary field illuminates with the first sidelobes the reflector, as depicted in Fig. 6. This illumination is defined at design level to match the required footprint size on ground.

Finally, it can be observed that the S/C and solar panels are second order while the crate is relevant at all frequencies and polarisations. Concerning the crate contribution, it was found that the scattering is due to the primary coupling among the feeds and the top floor while the reflector-crate double scattering is negligible.

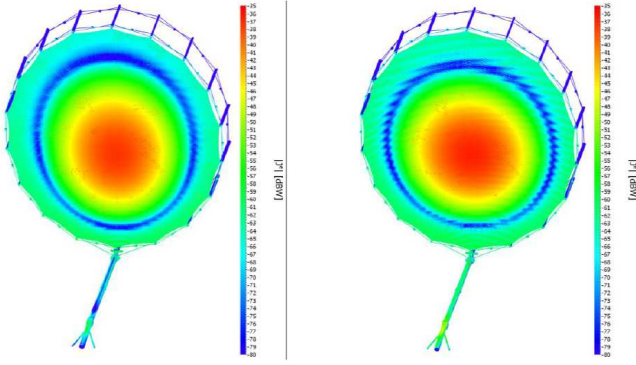


Fig. 6. Current distribution at X band on the reflector, truss and boom, H-pol on the left and V-pol on the right

Table 7 reports the total scattered power for the K- and Ka-band for the two polarisations. It is interesting to notice that in Ka-band the overall scattered power is approximately -28 dB, worst case, and therefore the impact of the scatterers in the overall antenna performance is marginal at this frequency.

TABLE 7: OVERALL SCATTERED POWER FOR V-POL AND H-POL IN K AND KA BAND

Scattered power [dB] vs Scatterers				
Scatterer	K band V-pol	K band H-pol	Ka band V-pol	Ka band H-pol
All scatterers	-22.15	-22.8	-28.17	-29.07

#### IV. CONCLUSIONS

A platform scattering analysis of the CIMR reflector antenna on the satellite was carried out over selected feeds at the center channel frequencies in L, C, X, K and Ka-bands. The effect of the truss, boom, crate, and satellite with solar panels was studied in vertical and horizontal polarisation by looking at the variations of the BE relative to the reflector antenna standalone.

Among the others, the evaluation of the BE was a key parameter because it impacts the final CIMR antenna temperature and the relative radiometric performance.

Moreover, a scattered power analysis was performed to compute the power scattered by each scatterer at all frequency bands to identify the most relevant for the scattering. It was found that boom and crate are the two objects which have the highest impact on the scattered power for all the frequencies, while the truss is not completely negligible at low frequencies, due to the higher primary illumination.

It was finally shown that the S/C body and solar panels have an almost negligible impact on the antenna performance for all the investigated frequencies.

#### REFERENCES

[1] S. Contu, R. Mizzoni, V. Lubrano, S. Varchetta, S. Endler, L. Datashvili, M. Grilli, B. Fiorelli, "CIMR Antenna S/S: An Overview,

Key Requirements And Challenges", 41st ESA Antenna Workshop, ESTEC, Noordwijk, The Netherlands, 2023

[2] V. Lubrano, R. Rigato, S. Contu, A. Montani, R. Mizzoni, G. Addamo, O. A. Peverini, G. Virone, C. Cappellin, P. G. Nicolaci, T. Rubæk, B. Fiorelli, "CIMR Antenna Sub-System Overall Design And Modelling", 41st ESA Antenna Workshop, ESTEC, Noordwijk, The Netherlands, 2023

[3] C. Cappellin, E. Jørgensen, P. Meincke, O. Borries, C. Nardini and C. Dreyer, "Detailed pattern computations of the UHF antennas on the spacecraft of the EXOMARS mission", 9th European Conference on Antennas and Propagation (EuCAP), Lisbon, Portugal, 2015

[4] GRASP/ESTEAM/QUPES/CHAMP3D/POS Software, TICRA, Copenhagen, Denmark [Online]. Available, [www.ticra.com](http://www.ticra.com).

[5] R. Mizzoni. "On the Beam Efficiency and Sidelobes of Radiometer Antennas"; submitted to European Conference on Antennas and Propagation (EuCAP), Glasgow, UK, 2024